Investigations of Electrochemically Active Regions in Bifunctional Air Electrodes Using Partially Immersed Platinum Electrodes

Atsunori Ikezawa[a], Kohei Miyazaki[a,b,*,z], Tomokazu Fukutsuka[a,*], and Takeshi Abe[a,*]

[a]*Graduate School of Engineering, Kyoto University, Nishikyo-ku, Kyoto 615-8510, Japan*

[b]*Japan Science and Technology Agency, 4-1-8 Honcho Kawaguchi, Saitama 332-0012, Japan*

* Electrochemical Society Active Member

[z] Corresponding Author: (E-mail) myzkohei@elech.kuic.kyoto-u.ac.jp

(FAX) +81-75-383-2488

Abstract

Oxygen reduction reaction (ORR) and oxygen evolution reactions (OER) on glassy-carbon-supported platinum electrodes (Pt/GCs), which are partially immersed in alkaline electrolytes, are investigated as a model of the triple phase boundary (TPB) in air electrodes for metal-air secondary batteries. ORR currents are measured with changing the vertical position of Pt/GCs, and OER currents are measured by linear sweep voltammetry. Based on the electrochemical results, it is found that thin liquid film on Pt/GCs effectively serves to expand TPB regions for ORR, but the liquid film hardly increases OER currents. Therefore, we conclude that the most effective TPB form are determined by the electrode reactions (ORR or OER), which are corresponding to discharge and charge processes for metal-air secondary batteries. In practice, it is strongly necessary to control the wettability of electrode inside, in order to construct high-performance bifunctional air electrodes.

Introduction

There has been increasing interest in metal-air secondary batteries such as zinc-air, aluminum-air, and iron-air secondary batteries.[1,2] These batteries potentially provide much higher energy densities than the current rechargeable batteries because they can utilize ambient air as their positive-electrode (air electrode) material. In addition, metal-air secondary batteries using aqueous electrolytes are also expected to satisfy the high safety standard because they can utilize non-flammable aqueous solutions. Therefore, they are attractive power sources for large-scale energy storages. However, there are some problems for practical use, for example, the dendrite formation in metal electrodes and the carbonation of alkaline electrolytes. Further, the large overpotential of air electrodes is one of the most serious problems to hinder the widely use of metal-air secondary batteries.[3]

In air electrodes, the electrochemical reactions (oxygen reduction (ORR) and oxygen evolution (OER)) occur only at the regions where three different species (electron, electrolyte, and oxygen gas) have contact with each other, so-called triple-phase boundary (TPB) regions. Therefore, TPB regions in air electrodes have significant influences on the overpotential and the power density of metal-air batteries. In order to construct air electrodes with better TPB regions, porous gas diffusion electrodes, which are composed of hydrophobic gas diffusion layers and mildly hydrophobic catalyst layers, have been used for air electrodes in metal-air secondary batteries (as shown in Fig. 1).[1,2] Porous electrodes have good feasibility for practical uses, but it is difficult to

investigate the intrinsic properties of the TPB regions by using such porous electrodes, because their microstructures are too complicated to be analyzed in detail. Therefore, partially immersed electrode systems had been applied for investigating of the properties of TPB regions as a model electrode (Fig. 2). [3-14] Mass transports of the ions and gases in the catalyst layers can be simulated in the partially immersed electrode system. In this system, ion transportation can be limited within thin liquid films, which cover the electrode surface. Reactant gases can permeate through thin liquid films to proceed electrochemical reactions on electrode surfaces. Therefore, the partially immersed electrode system allows controlling the electrode environment to shed lights on how TPB regions effectively work in bifunctional air electrodes.

Most of previous reports using these systems have dealt with acid electrolytes, which were utilized for proton-exchange membrane fuel cells, phosphoric acid fuel cells, etc. [3-11] There are a few reports that have dealt with alkaline electrolytes[13,14], but there is little information on the influences of various conditions (such as electrolyte concentrations, oxygen partial pressures, and electrode wettability) on TPB regions. In addition, OER, that is the charging process for air electrodes, has not been examined by the model electrode.

In this study, we revisited the partially immersed electrodes in order to investigate ORR and OER as a model of the TPB regions in air electrodes for metal-air secondary batteries.

Experimental

Preparation of Pt/GC electrodes

A mirror polished glassy carbon plate (GC, 10.0 × 20.0 × 1.2 mm, Tokai Carbon Co. Ltd., GC-SS20) was employed as a substrate. The GC plate was pretreated by cyclic voltammetry in an aqueous solution of 1.0 mol dm^{-3} HNO_3 saturated with Ar gas in a potential range of −0.147 − 1.003V (vs. Ag/AgCl) (namely, 0.050 − 1.200 V (vs. SHE)) for 10 cycles, and Pt particles were deposited by galvanostatic pulse deposition or D.C. sputtering. In the galvanostatic pulse deposition, an electrochemical two-electrode cell was used. An aqueous solution of 1 mmol dm^{-3} H_2PtCl_6 and 2.1 mmol dm^{-3} HCl saturated with Ar gas was used as an electrolyte. The pretreated GC plate was immersed to the electrolyte by half as the working electrode, and Pt wire was used as a counter electrode. Electrodeposition was carried out under Ar atmosphere with current pulses from a voltammetry system (Bio-Logic, SP-150m); pulse current density: 4.0 mA cm^{-2}, pulse width: 0.1 s, interval period: 0.5 s, pulse cycles: 10 or 30 times. In the D.C. sputtering, the pretreated GC plate was set in a sample holder masking the half of the GC (10 × 10 mm), and platinum layer was deposited on the exposed part of the GC surface by D.C. sputtering apparatus (Osaka Vacuum, OVS-350) for 5 min. Hereafter, we call these electrodes Pt/GCs.

Surfaces of the electrodes were observed by scanning electron microscopy (Hitachi, S-3000H). Contact angles of solutions of 1.0 mol dm^{-3} KOH on the electrodes were evaluated using a contact angle meter (KYOWA, DM-301) in order to determine their wettability.

Cyclic voltammetry of Pt/GCs in a solution of 0.5 mol dm^{-3} H_2SO_4 was carried out using an electrochemical three-electrode cell that consisted of Pt/GCs, Ag/AgCl (with a double junction), and

Pt wire were used as a working, reference, and counter electrodes, respectively.

Electrochemical measurements for partially immersed Pt/GCs

Pt/GCs were set at one end of a stainless steel rod as a working electrode. The other end of the stainless steel rod was attached to a micrometer, and the height of the electrode was adjusted using the micrometer within accuracy of ± 0.01 mm. In electrochemical measurements, Pt deposited areas of Pt/GCs were fully immersed, then Pt/GCs were raised by the micrometer head (Fig. 3). A Hg/HgO electrode (with a double junction) was used as a reference electrode, and Pt wire was used as a counter electrode. Aqueous solutions of 0.10 − 10 mol dm^{-3} KOH (saturated with mixed gases of O_2 and Ar at given ratios) was used as electrolytes. Electrochemical measurements were carried out under the mixed gases at the same ratios for KOH solutions.

Theoretical treatment

We performed theoretical treatment using a similar model reported by Bennion and Tobias.[14] Figure 4 shows schematic illustration of the partially immersed Pt/GC used in the calculation. For the sake of simplicity, it was assumed that there were two surface regions of Pt/GC: a fully immersed region (length: l') and a uniform thin liquid film (length: l, thickness: δ_{film}). An intrinsic meniscus region was incorporated into the fully immersed region. Given that the potential

drop in the thin liquid film obeys Ohm's law, they can be described by the following equation (see List of symbols),

$$\frac{\partial \eta}{\partial y} = \frac{J}{\kappa W \delta_{\text{film}}} \quad [1]$$

When the rate determining step of ORR is the charge transfer process, the local current density i can be described by the following Butler-Volmer equation,

$$i = i_0 \left\{ -\frac{C_{O_2}(0,t)}{C_{O_2}} \exp\left(-\frac{4\alpha F \eta}{RT} \right) + \frac{C_{OH^-}(0,t)}{C_{OH^-}} \exp\left(\frac{4(1-\alpha) F \eta}{RT} \right) \right\} \quad [2]$$

$$i_0 = FAk^0 C_{O_2}^{1-\alpha} C_{OH^-}^{\alpha} \quad [3]$$

When the rate determining step of ORR is the transport of oxygen, the local current density i can be described by Fick's first law,

$$i = -4FD_{O_2} \left(\frac{\partial C_{O_2}(0,t)}{\partial x} \right) \quad [4]$$

Assuming that the oxygen diffusion process is first-order and linear, we have following equation by integration of Eq. [4],

$$C_{O_2}(0,t) = C_{O_2} - \frac{i \delta_{\text{film}}}{4FD_{O_2}} \quad 5]$$

Given that the OH^- concentrations are uniform in the thin liquid film, we have the following equation,

$$C_{OH^-}(0,t) = C_{OH^-} \quad [6]$$

Substituting Eqs. [5] and [6] to Eq. [2], the local current density i can be described by the following equation,

$$i = \frac{i_0\left\{-\exp\left(-\frac{4\alpha F\eta}{RT}\right)+\exp\left(\frac{4(1-\alpha)F\eta}{RT}\right)\right\}}{1-\frac{i_0\delta_{\text{film}}}{4FD_{O_2}C_{O_2}}\exp\left(-\frac{4\alpha F\eta}{RT}\right)} \qquad [7]$$

The local ionic current J was linked with the local current density i as follows,

$$\frac{\partial J}{\partial y} = i \qquad [8]$$

Solving [1], [7], and [8] numerically, we simulated current distributions on the partially immersed Pt/GCs. Boundary conditions were set to the following equations,

$$y = 0;\ \ \eta = E \qquad [9]$$

$$y = l;\ \ J = i \qquad [10]$$

At the fully immersed area, the local current density i can be calculated only from Eq. [7], and the thickness of the thin liquid film δ_{film} is replaced with the steady state thickness of the diffusion layer δ_{dl}.

Results and Discussion

Characterization of Pt/GC electrodes

Figure 5 shows SEM images of the surfaces of Pt/GCs made by the galvanostatic pulse deposition and D.C. sputtering. Pt particles prepared by the galvanostatic pulse deposition, having mean grain diameters of about 100 and 200 nm for 10 and 30 potential pulses, respectively, were sparsely deposited on the surface of GC supports. In contrast, Pt fine particles wholly covered the GC support in the case of D.C. sputtering.

Hydrophilic/hydrophobic properties of Pt/GCs electrodes were measured by the contact angles for a drop of KOH solution. As summarized in Table 1, the surfaces of Pt/GCs became more hydrophilic with the increase of the densities of Pt particles on GCs. Two reasons are responsible for the increase in wettability caused by Pt deposition[10]: an increase in surface roughness by Pt deposition, and the hydrophilic nature of deposited Pt particles.

Figure 6 shows cyclic voltammograms of Pt/GCs in the 10th cycle. Characteristic redox peaks of Pt were observed, which can be ascribed to the hydrogen adsorption and desorption peaks at lower potentials and the oxidation film formation and dissociation peaks at higher potentials. Electrochemical surface areas (ECSA) of Pt/GC electrodes were calculated based on the following equation, and resulted values are shown in the inset of Fig. 6,

$$\mathrm{ECSA} = \frac{C_{\mathrm{Hdis}}}{210} \qquad [11]$$

Dependence of KOH concentrations

Figure 7 shows ORR currents at −0.524 V (vs. Hg/HgO) (0.400 V (vs. RHE)) as a function of the electrode position of partially immersed Pt/GCs made by pulse deposition (30 times) in KOH solutions. Oxygen partial pressure was set at 1.013×10^5 Pa (1 atm). An electrode position (h = 0 mm) means the setting where the electrode area with Pt particles was fully immersed (Fig. 3). At around this position, ORR currents were quite lessened when KOH concentrations were 5 and 10 mol dm^{-3}, due to the lower oxygen transportation as shown in Table 2. In any concentrations, ORR

currents were nearly constant up to the position of *ca*. 1.0 mm. This result indicates that the intrinsic meniscuses were formed along the electrode up to 1.0 mm. Intrinsic meniscus had thick liquid film that have few positive effects to increase ORR currents.[11] At the electrode position higher than 1.0 mm, drastic increases in ORR currents were observed. This suggests that thin liquid film was formed on Pt/GCs, and effective TPB region was raised above the intrinsic meniscus. Followed by the rapid increase in ORR currents, the currents approached to the constant values, which indicate that effective TPB regions were restricted in a limited height range of thin liquid films. Furthermore, we found that the lengths of effective TPB regions were dependent on the concentration of electrolytes; the effective TPB lengths were more raised with an increase in ion conductivities. Therefore, we had notion that effective TPB regions were regulated by the ohmic potential drops of ion transport in thin liquid film.

In the case of 10 mol dm^{-3} KOH, the currents were completely lower than those in other concentrations. As shown in Table 2, oxygen transport through 10 mol dm^{-3} KOH solution was significantly restricted, thus the currents for ORR were quite lower. In practical metal-air batteries, the concentrations of electrolyte solutions were set at 5.0 − 7.0 mol dm^{-3} KOH because of their relatively higher ion conductivities.[18] However, such concentrated alkaline electrolytes generally have fairly low oxygen transport properties. Therefore, as shown in Fig. 7, quite low currents were observed at the fully immersed position in 5.0 mol dm^{-3} KOH. In contrast, much higher currents were observed at positions where thin liquid films were formed adequately on the electrode surface

as an electrolyte. This indicates that the formation of thin liquid films is very important to construct TPB regions in air electrodes.

Influence of oxygen partial pressures

Figure 8a shows the variations of ORR currents of partially immersed Pt/GCs (made by pulse deposition for 30 times) at −0.524 V (vs. Hg/HgO) (0.400 V (vs. RHE)) and given electrode positions in a solution of 1.0 mol dm^{-3} KOH under various oxygen partial pressures. Currents were proportional to oxygen partial pressures at h = 0 mm, since oxygen solubilities in the electrolytes were proportional to oxygen partial pressures obeying Henry's law.[19] By comparison of the height where the currents approached to the constant values, the height became slightly greater with the decrease in oxygen partial pressures; it was *ca.* 4 mm at 1.0 atm, 5 mm at 0.2 atm. This is probably because the higher oxygen partial pressures caused larger ORR currents, resulted in bigger ohmic losses. In contrast to the currents at h = 0 mm, the currents at higher positions were linear but not directly proportional to oxygen partial pressures as shown in Fig. 8b. The difference in the intercepts could be caused by the enhanced oxygen transportation at TPB region, because of the short diffusion distance of oxygen through thin liquid film.

Influence of the Pt loadings

Figure 9 shows the variations of ORR current densities (normalized by geometrical areas) at −0.524 V (vs. Hg/HgO) (0.400 V (vs. RHE)) with electrode position in a solution of 1.0 mol dm^{-3} KOH. Oxygen partial pressure was kept at 1.013×10^5 Pa (1 atm). The length of thin liquid film effective for ORR became longer with an increase in the amount of deposited Pt. This is because that Pt/GC with more Pt deposits had higher wettability and thicker liquid film was formed on the electrode surface. This suggests that changing electrode wettabilities should be one of the possible ways to optimize thin liquid film thickness.

Oxygen evolution reactions on Pt/GCs

Figure 10 shows linear sweep voltammograms of OER on Pt/GCs made by 30 times pulse deposition. In contrast to ORR, OER currents at the fully immersed position were larger than those at the partially immersed positions, regardless of KOH concentration. Therefore, the fully immersed electrode worked better than thin liquid film for OER, and it was suggested that a flooded catalyst layer in practical air electrodes should be preferable for OER. Generally, gas evolution electrodes suffer from gas bubble plugging, which prevents reactant ions from accessing the electrode surface.[20] Therefore, pore size and distribution of air electrodes should be taken into account for smooth removal of evolved oxygen bubbles.

Based on the above results, it is implied that ORR and OER undertake in different regions of bifunctional air electrodes, and two reactions have different requirements for electrochemical

environments in order to operate effectively. Therefore, it is necessary to control the electrolyte wettability of the electrodes and to construct bifunctional air electrodes with a combination of wet and flooded regions for discharging and charging processes, respectively.

AC impedance measurement

In order to determine ionic resistances of thin liquid films, A.C. impedance measurements were carried out. Nyquist plots of Pt/GCs made by 30 pulses in aqueous solutions of 1.0 and 5.0 mol dm^{-3} KOH saturated with Ar gas were shown in Fig. 11. Applied A.C. amplitude was set to 50 mV. Pt/GCs were held at h = 0, 10, and 12 mm. Transmission line type (TML) frequency dependences were observed in the Nyquist plots. These TML frequency dependences were widely seen in electrochemical systems in which ionic transportation was restricted in a confined space; for example, flat metal electrodes covered with thin liquid films.[21] We carried out curve fitting using an equivalent circuit and a commercially available program (Z-view) in order to determine the resistances of thin liquid film. Impedance of the electrode area covered with thin liquid film (Z_{film}) can be described by the following equation

$$Z_{\mathrm{film}} = \frac{R_{\mathrm{film}}}{\Lambda^{1/2}} \coth\left(\Lambda^{1/2}\right) \qquad [12]$$

where Λ is the dimensionless admittance of the electrode area covered with thin liquid film and described by the following equation, [22]

$$\Lambda = \frac{l^2}{Z_{\mathrm{el}} \kappa \delta_{\mathrm{film}}} \qquad [13]$$

In this case, the specific impedance of the interface between the electrode and the thin liquid film (Z_{el}) can be described by following equation,

$$Z_{\mathrm{el}} = \frac{1}{\frac{1}{R_{\mathrm{ct}}} + (\mathrm{j}\omega)^{\phi} T_{\mathrm{CPE}}} \qquad [14]$$

Fitted curves were shown in Fig. 12, and the resistances of thin liquid films were calculated to be 9.6 ± 0.6 and 3.7 ± 0.1 kΩ in aqueous solutions of 1.0 and 5.0 mol dm^{-3} KOH, respectively. These large resistances were the cause of ohmic potential drops in thin liquid films. Given that the ion conductivity of the thin liquid film is the same as that of the bulk electrolyte solution, the film thickness δ_{film} can be estimated by following equation.

$$R_{\mathrm{film}} = \frac{1}{\kappa \delta_{\mathrm{film}} W} \qquad [15]$$

The film thicknesses were estimated to be 2.2 ± 0.1 and 2.4 ± 0.1 μm in aqueous solutions of 1.0 and 5.0 mol dm^{-3} KOH, respectively.

Theoretical results and comparison with experimental results

We simulated polarization curves of partially immersed Pt/GCs using a simple model. The physical properties used in the simulation were shown in Table 3. Figure 13 shows the measured and simulated polarization curves for ORR on Pt/GCs made by 30 pulses. Simulated curves were almost the same as the measured curves in all cases. Therefore, it is shown that the model including the

large resistances of thin liquid films was reasonable and supported the notion that the ohmic potential drops in thin liquid film dominantly regulated TPB regions in air electrodes.

Conclusion

ORR and OER on partially immersed Pt/GCs were investigated as model of bifunctional air electrodes for metal-air secondary batteries. It was shown that partially immersed Pt/GCs served as a useful model electrode. In addition, it should be noted that the thin liquid film works as a good triple phase boundary for ORR while the fully immersed electrode works as a good TPB for OER. Therefore, optimizing electrolyte wettability and forming adequate amounts of thin liquid films and flooded areas in catalyst layer will lead to some improvement of the over potential and the power density of air electrodes.

List of symbols

C_{Hdis} [C]	Electric quantity of the hydrogen desorption reaction
$C_{\mathrm{O_2}}(0,t)$ [mol cm^{-3}]	Concentration of O_2 at the electrode/electrolyte interface
$C_{\mathrm{OH^-}}(0,t)$ [mol cm^{-3}]	Concentration of OH^- at the electrode/electrolyte interface
$C_{\mathrm{O_2}}$ [mol cm^{-3}]	Concentration of O_2 at bulk electrolyte
$C_{\mathrm{OH^-}}$ [mol cm^{-3}]	Concentration of OH^- at bulk electrolyte
$D_{\mathrm{O_2}}$ [mol cm^{-1} s^{-1}]	Diffusion coefficient of O_2
E [V]	Applied potential
F [C mol^{-1}]	Faraday constant
i [A cm^2]	Local current density
i_0 [A cm^2]	Exchange current density
J [A]	Local ionic current
k^0 [cm s^{-1}]	Standard rate constant
l [cm]	Length of the electrode area covered with the thin liquid film
l' [cm]	Length of the electrode area fully immersed and covered with the intrinsic meniscus
ϕ	CPE exponent at the electrode areas covered with the thin liquid film
$P_{\mathrm{O_2}}$ [Pa]	Partial pressure of oxygen in the cell
R [J K^{-1} mol^{-1}]	Gas constant
R_{ct} [Ω cm^2]	Specific resistance of charge transfer at the thin liquid film

R_{film} [Ω]	Ionic resistance of the thin liquid film
T [K]	Absolute temperature
T_{CPE} [F cm^{-2}]	Specific CPE constant at the electrode areas covered with the thin liquid film
W [cm]	Width of the Pt/GC
Z_{el} [Ω cm^{2}]	Specific impedance of the interface between the electrode and the thin liquid film
Z_{film} [Ω]	Impedance of the electrode area covered with a liquid thin film
α	Symmetry factor of ORR
δ_{dl} [cm]	Steady state thickness of the diffusion layer
δ_{film} [cm]	Thickness of the thin liquid film
η [V]	Local overpotential
κ [S cm^{-1}]	Ion conductivity
Λ	Dimensionless admittance of the electrode area covered with the liquid thin film

References

1. F. Cheng, J. Chen, *Chem. Soc. Rev.*, **41**, 2172 (2012).

2. L. Jörissen, *J. Power Sources,* **155**, 23 (2006).

3. H. Arai, S. Miller, O. Haas, *J. Electrochem. Soc.*, **147**, 3584 (2000).

4. F. G. Will, *J. Electrochem. Soc.*, **110**, 145 (1963).

5. F. G. Will, *J. Electrochem. Soc.*, **110**, 152 (1963).

6. H. J. R. Maget, R. Roethlein, *J. Electrochem. Soc.*, **112**, 1034 (1965).

7. R. J. Roethlein, H. J. R. Maget, *J. Electrochem. Soc.*, **113**, 581 (1966).

8. E. N. Lightfoot, *J. Electrochem. Soc.*, **113**, 614 (1966).

9. E. N. Lightfoot, *J. Electrochem. Soc.*, **113**, 1325 (1966).

10. M. Matsumura, J. R. Selman, *J. Electrochem. Soc.*, **139**, 1255 (1992).

11. M. Inaba, M. Uno, J. Maruyama, A. Tasaka, K. Katakura, Z. Ogumi, *J. Electroanal. Chem.*, **417**, 105 (1996).

12. T. Kinumoto, Y. Uchimoto, X. Ming, K. Katakura, K. Kikuchi, Y. Iriyama, T. Abe, M. Inaba, Z. Ogumi, *Electrochemistry*,**75**, 248 (2007).

13. D. N. Bennion, C. W. Tobias, *J. Electrochem. Soc.*, **113**, 589 (1966).

14. D. N. Bennion, C. W. Tobias, *J. Electrochem. Soc.*, **113**, 593 (1966).

15. R. H. Muller, *J. Electrochem. Soc.*, **113**, 943 (1966).

16. R. E. Davis, G. L. Horvath, C. W. Tobias, *Electrochim. Acta*, **12**, 287 (1967).

17. R. J. Gilliam, J. W. Graydon, D. W. Kirk, S. J. Thorpe, *Int. J. Hydrogen Energy,* **32**, 359 (2007).

18. J.-S. Lee, S. T. Kim, R. Cao, N.-S. Choi, M. Liu, K. T. Lee, J. Cho, *Adv. Energy. Mater.,* **1**, 34 (2011).

19. R. Sander, *Atmos. Chem. Phys. Discuss.,***14**, 29615 (2014).

20. M. M. Saleh, *Electrochim. Acta*, **45**, 959 (1999).

21. A. Nishikata, Y. Ichihara, T. Tsuru, *Corros. Sci.*, **37**, 897 (1995).

22. A. Lasia, in *Modern Aspects of Electrochemistry*, M. Schlesinger, Ed., Vol. 43, Springer, Berlin (2009)

23. F. H. B. Lima, E. A. Ticianelli, *Electrochim. Acta*, **49**, 4091 (2004).

Figure captions

Figure 1. Schematic illustration of a gas diffusion electrode.

Figure 2. Schematic illustration of a partially immersed electrode.

Figure 3. Schematic illustration of partially immersed electrodes with thin liquid films.

Figure 4. Schematic illustration of the partially immersed Pt/GC used in the calculation.

Figure 5. SEM images of Pt/GC prepared by (a) 10 and (b) 30 pulses, and (c) sputtering.

Figure 6. Cyclic voltammograms of Pt/GC in an aqueous solution of 0.5 mol dm^{-3} H_2SO_4. Pt/GCs were prepared by (a) 10 pulses, (b) 30 pulses, and (c) sputtering.

Figure 7. Oxygen reduction currents of Pt/GC at −0.524 V (vs. Hg/HgO) in various KOH solutions plotted against electrode positions.

Figure 8. Oxygen reduction currents of Pt/GC at −0.524 V (vs. Hg/HgO) in 1.0 mol dm^{-3} KOH solution under various O_2 partial pressures plotted against electrode position.

Figure 9. Oxygen reduction currents of various Pt/GCs at −0.524 V (vs. Hg/HgO) in 1.0 mol dm^{-3} KOH solutions plotted against electrode positions.

Figure 10. Linear sweep voltammograms of Pt/GC in (a) 1.0 and (b) 5.0 mol dm^{-3} KOH solutions saturated with O_2 gas.

Figure 11. Nyquist plots of Pt/GCs (30 pulses) in aqueous solutions of (a) 1.0 and (b) 5.0 mol dm^{-3} KOH saturated with Ar gas.

Figure 12. Measured and calculated Nyquist plots of Pt/GCs made by 30 pulses in aqueous solutions

of (a) 1.0 and (b) 5.0 mol dm^{-3} KOH saturated with Ar gas. Pt/GCs were held at h = 12 mm. (c) An equivalent circuit used for fitting.

Figure 13. Measured (a,b) and simulated (c,d) polarization curves for ORR on Pt/GCs made by 30 pulses (a),(c) in 1.0 and 5.0 mol dm^{-3} KOH solutions saturated with O_2 and (b),(d) in 1.0 mol dm^{-3} KOH under various oxygen partial pressures. Pt/GCs were held at h = 10 mm.

Table 1. Contact angles for 1.0 mol dm^{-3} KOH drops on Pt/GCs

	Sputtering	30 pulses	10 pulses
Contact angle / º	67	86	91

Table 2. Products of oxygen diffusion coefficient D_{O2} and oxygen solubility C_{O2} and conductivities κ of KOH solutions

KOH conc. / M	$D_{O2}C_{O2}\times 10^{11}$ / mol cm^{-1} s^{-1}	Reference	κ / S cm^{-1}	Reference
0.1	1.8	[16]	0.024	[17]
1.0	1.2	[16]	0.215	[17]
5.0	0.13	[16]	0.612	[17]
10	0.01	[16]	0.533	[17]

Table 3. Physical properties used in the calculation

Symbol	Name	Value
k^0	Standard rate constant	8.1×10^{-12} cm s^{-1} (1.0 mol dm^{-3}) 1.2×10^{-11} cm s^{-1} (5.0 mol dm^{-3})
$\frac{4\alpha F}{RT}$	Tafel slope	27 mV ($\eta \leq 0.1$ V) 53 mV ($\eta > 0.1$ V) [23]
D_{O_2}	Oxygen diffusion coefficient	[16]
C_{O_2}	Oxygen solubility	[16]
W	Film width	2.0 cm
κ	Electrolyte conductivity	[17]
F	Faraday constant	96485 C mol^{-1}
δ_{film}	Film thickness	2.4 μm (1.0 mol dm^{-3}) 2.2 μm (5.0 mol dm^{-3})
δ_{dl}	Steady state diffusion layer thickness	220 μm
l	Film length	0.8 cm
l'	Fully immersed and intrinsic meniscus length	0.2 cm

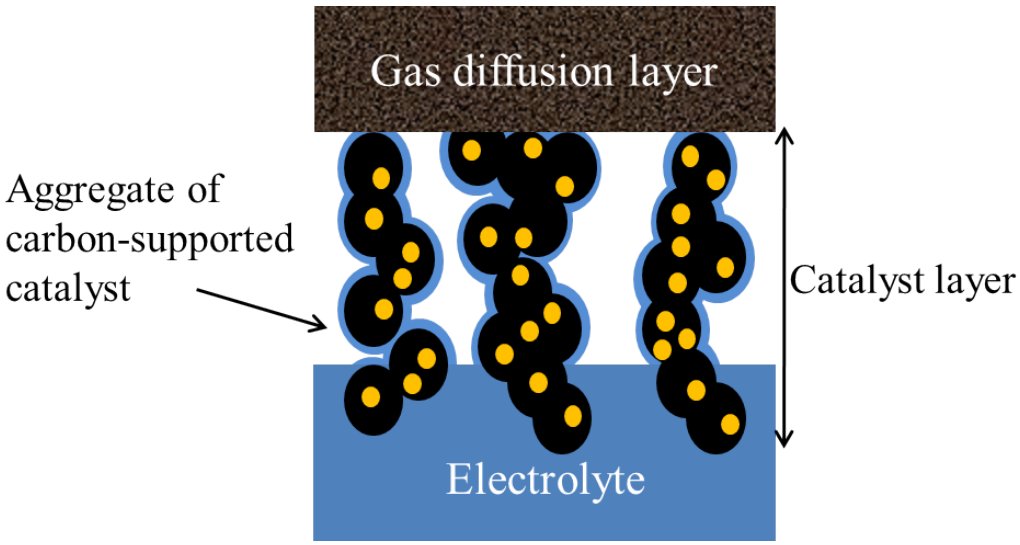

Figure 1. Schematic illustration of a gas diffusion electrode.

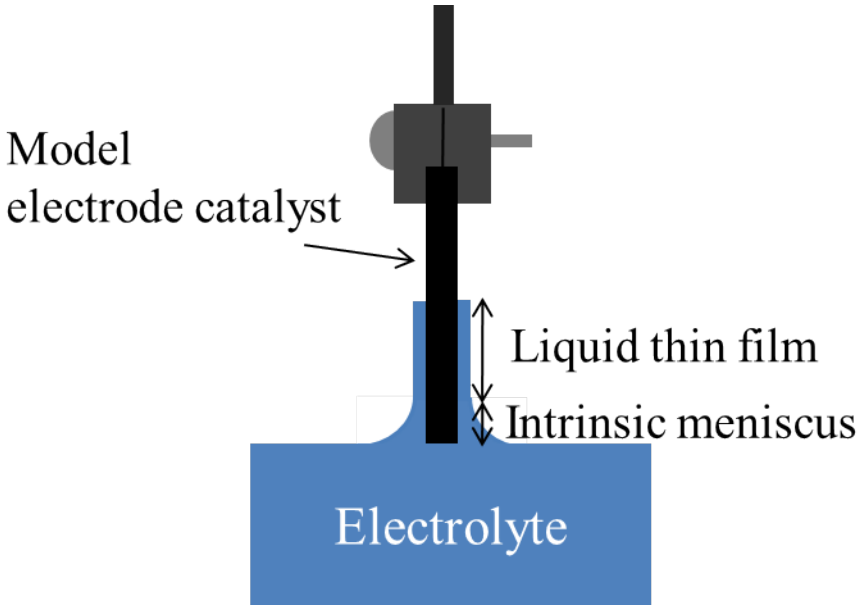

Figure 2. Schematic illustration of a partially immersed electrode.

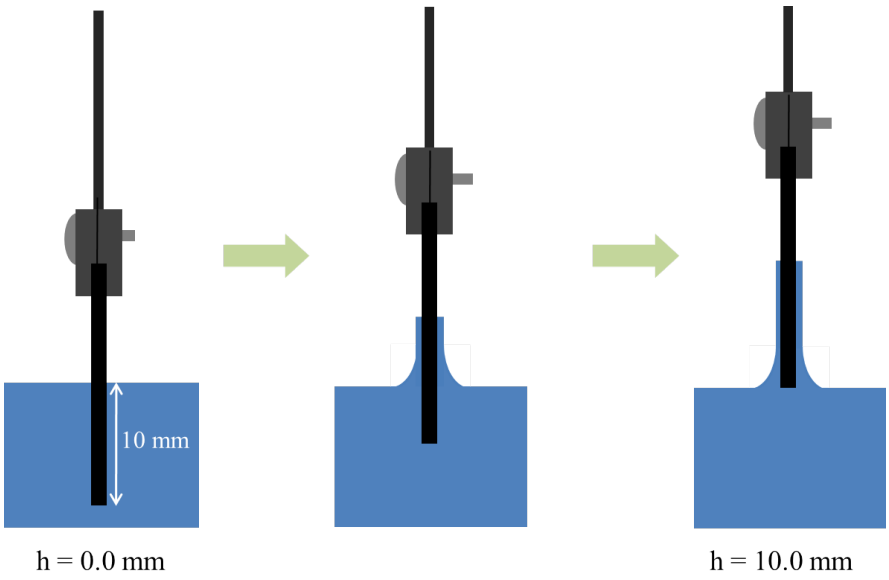

Figure 3. Schematic illustration of partially immersed electrodes with thin liquid films.

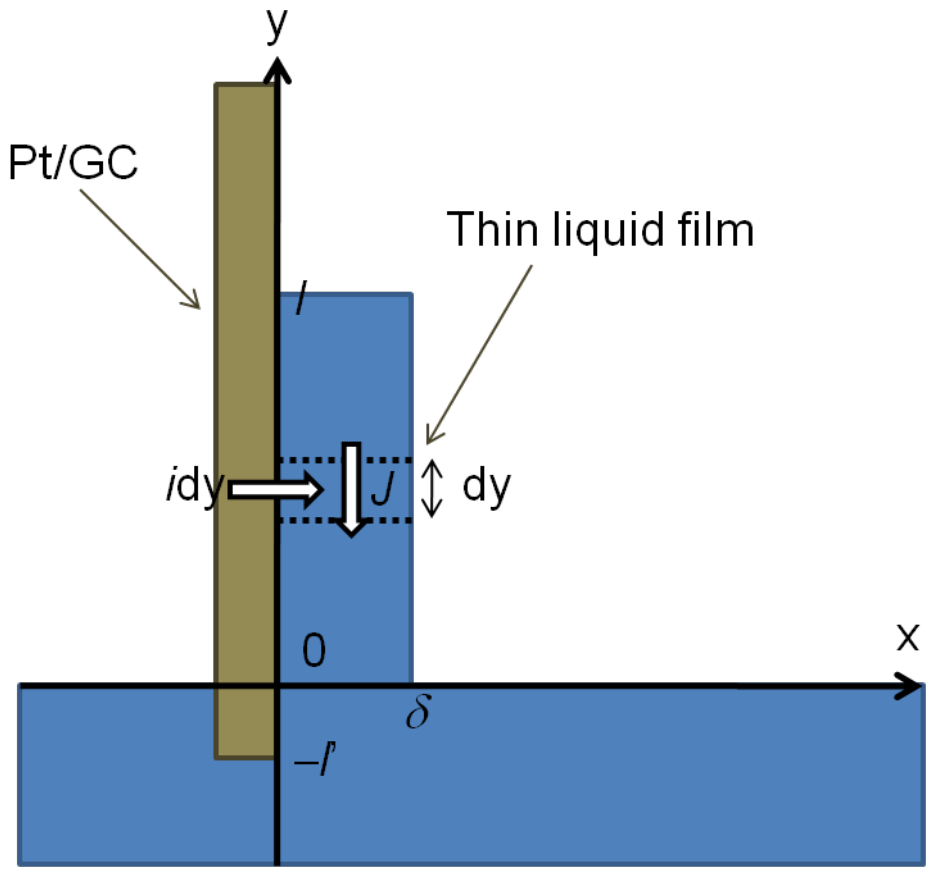

Figure 4. Schematic illustration of the partially immersed Pt/GC used in the calculation.

(a) 10 pluses

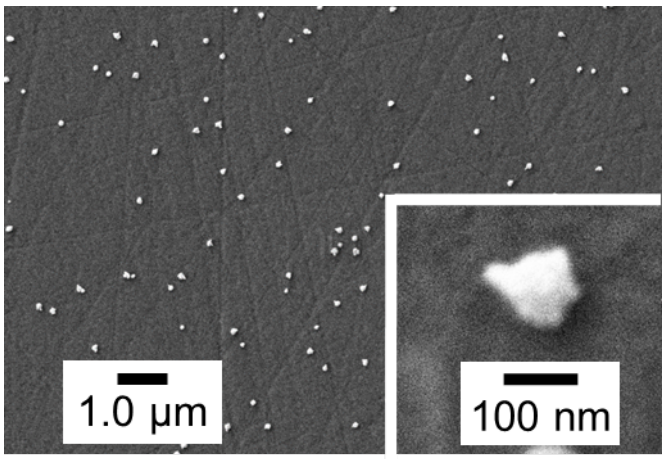

(b) 30 pluses

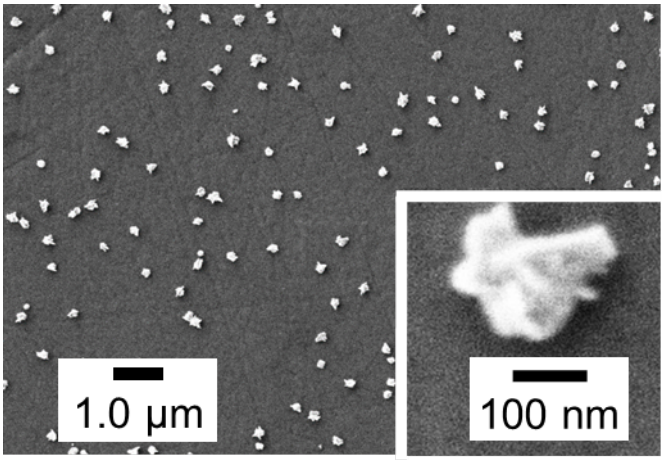

(c) Sputtering

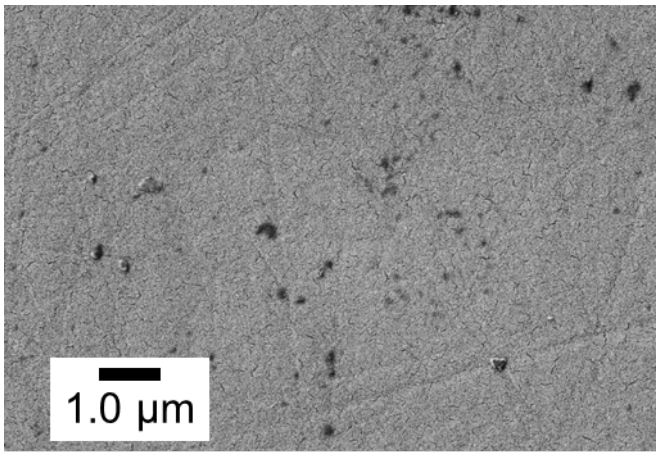

Figure 5. SEM images of Pt/GC electrodes prepared by (a) 10 and (b) 30 pulses, and (c) sputtering.

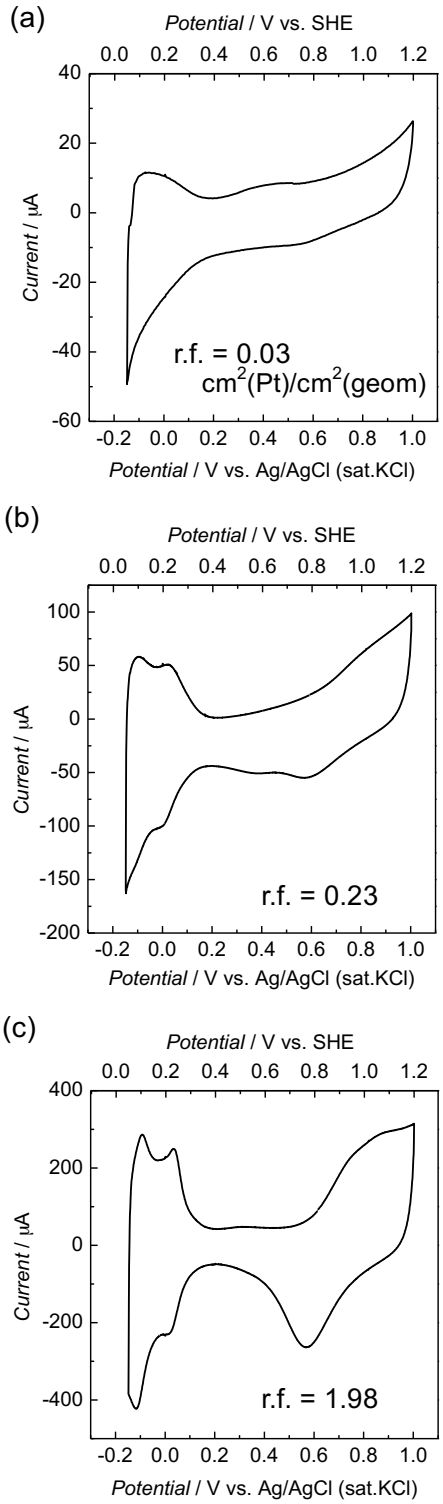

Figure 6. Cyclic voltammograms of Pt/GC in an aqueous solution of 0.5 mol dm^{-3} H_2SO_4. Pt/GCs were prepared by (a) 10 pulses, (b) 30 pulses, and (c) sputtering.

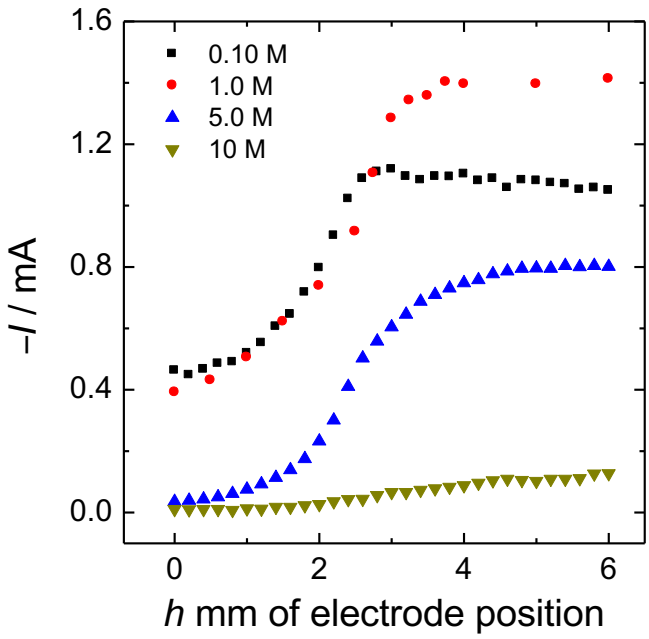

Figure 7. Oxygen reduction currents of Pt/GC at −0.524 V (vs. Hg/HgO) in various KOH solutions plotted against electrode positions.

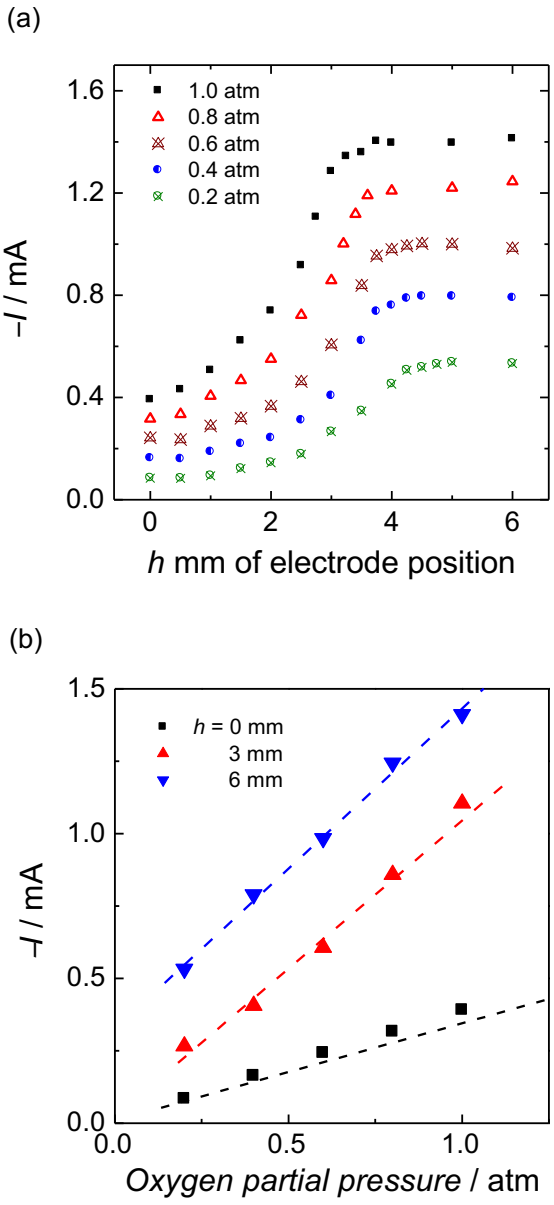

Figure 8. (a) Oxygen reduction currents of Pt/GC at −0.524 V (vs. Hg/HgO) in 1.0 mol dm^{-3} KOH solution under various O_2 partial pressures plotted against electrode position. (b) The dependence of oxygen partial pressure.

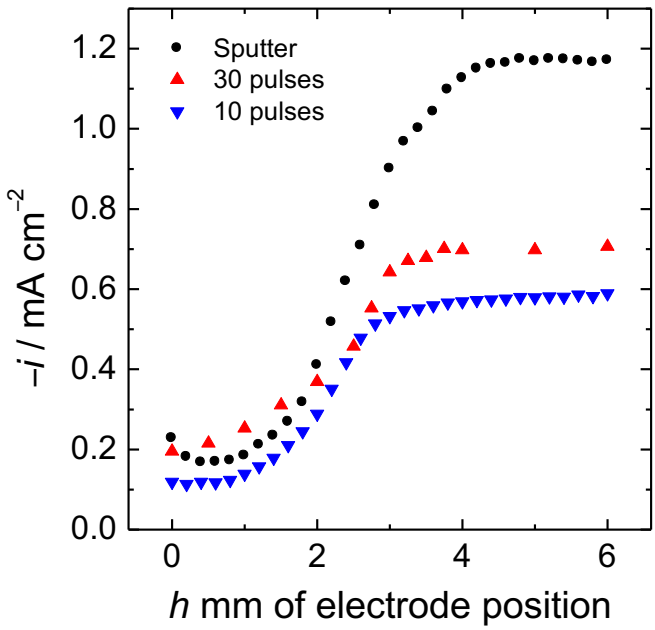

Figure 9. Oxygen reduction currents of various Pt/GCs at −0.524 V (vs. Hg/HgO) in 1.0 mol dm^{-3} KOH solutions plotted against electrode positions.

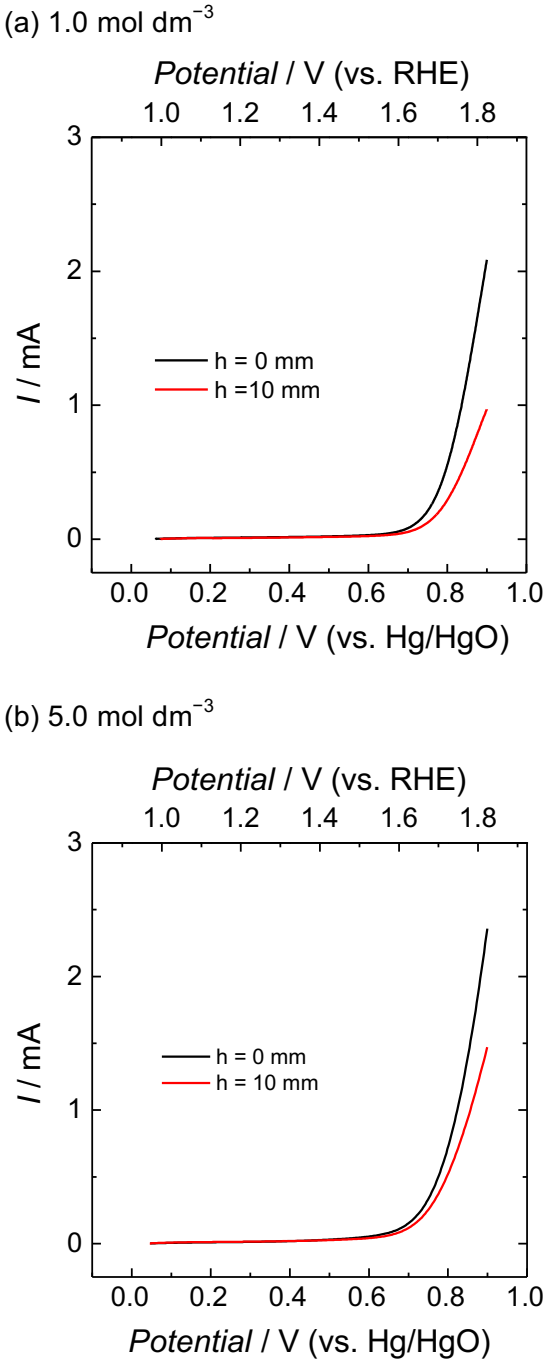

Figure 10. Linear sweep voltammograms of Pt/GC in (a) 1.0 and (b) 5.0 mol dm^{-3} KOH solutions saturated with O_2 gas.

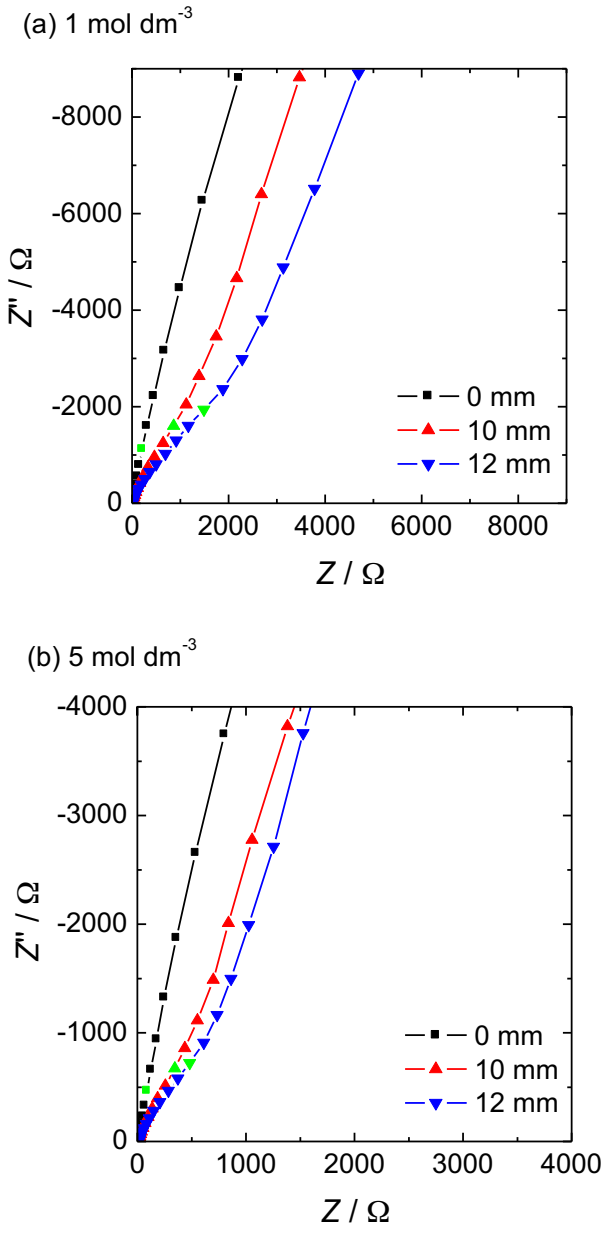

Figure 11. Nyquist plots of Pt/GCs (30 pulses) in aqueous solutions of (a) 1.0 and (b) 5.0 mol dm^{-3} KOH saturated with Ar gas.

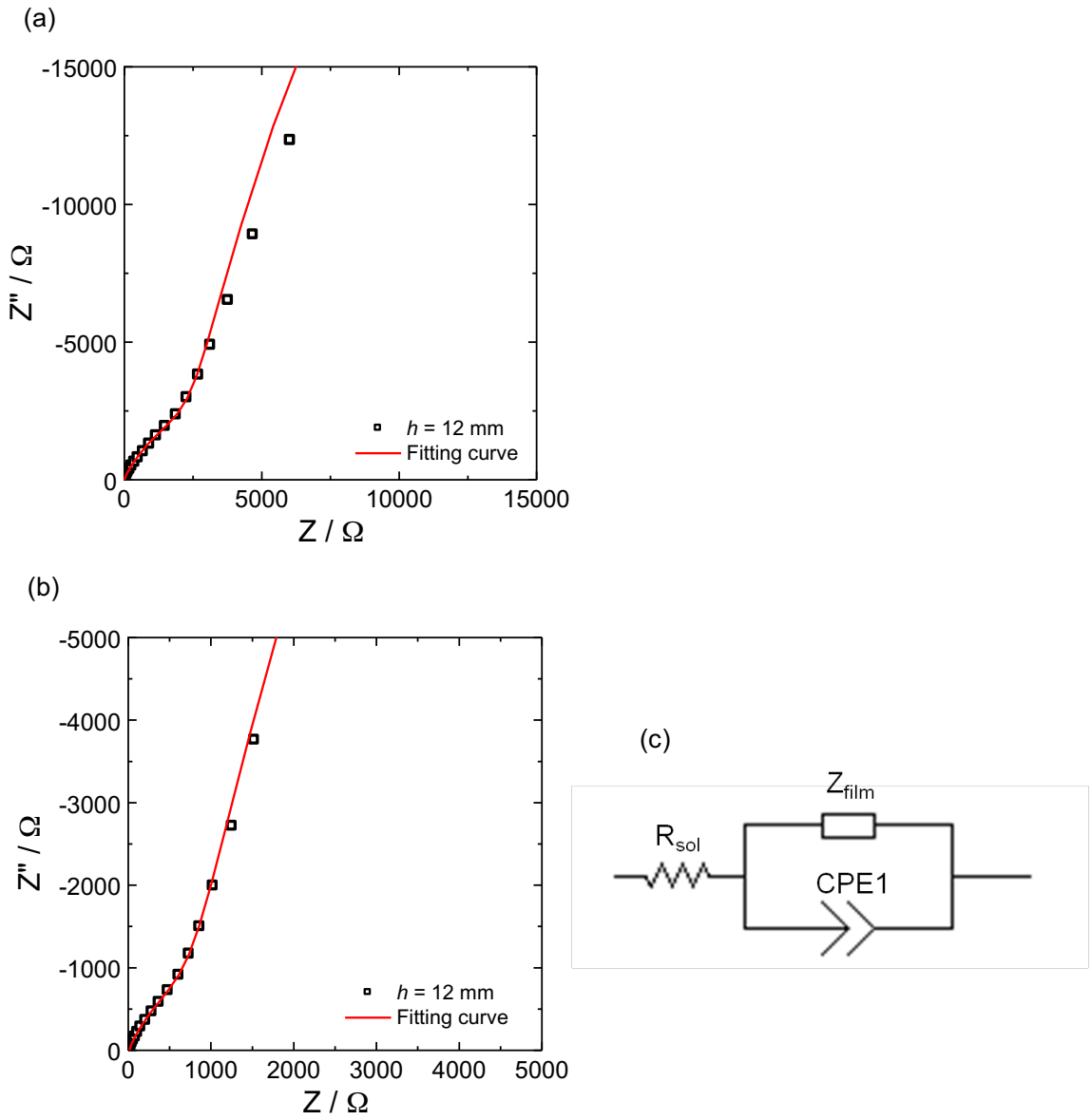

Figure. 12. Measured and calculated Nyquist plots of Pt/GCs made by 30 pulses in aqueous solutions of (a) 1.0 and (b) 5.0 mol dm^{-3} KOH saturated with Ar gas. Pt/GCs were held at h = 12 mm. (c) An equivalent circuit used for fitting.

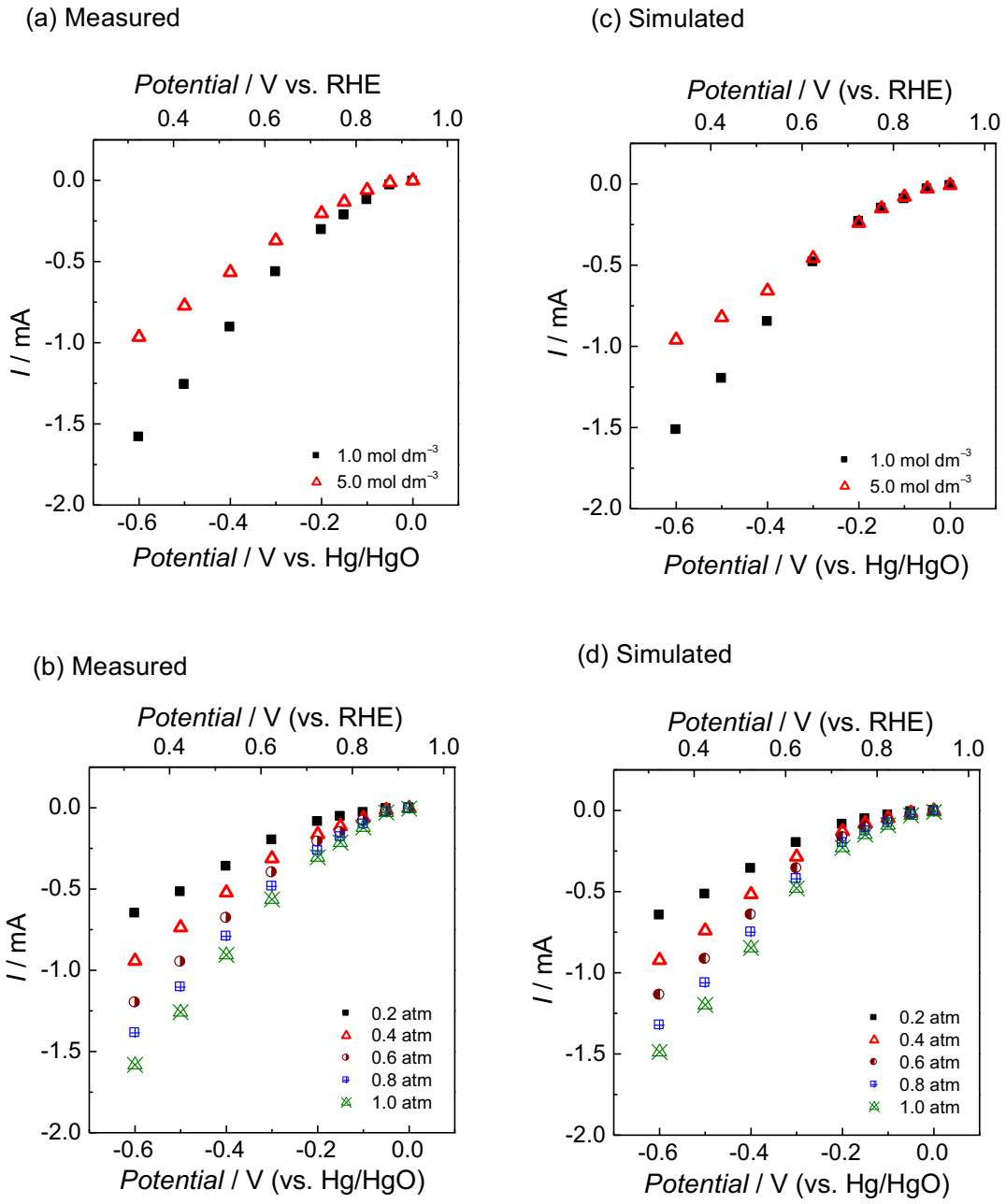

Figure 13. Measured (a,b) and simulated (c,d) polarization curves for ORR on Pt/GCs made by 30 pulses (a),(c) in 1.0 and 5.0 mol dm^{-3} KOH solutions saturated with O_2 and (b),(d) in 1.0 mol dm^{-3} KOH under various oxygen partial pressures. Pt/GCs were held at h = 10 mm.